HHS Public Access

Author manuscript

Dev Biol. Author manuscript; available in PMC 2019 November 15.

Published in final edited form as:

Dev Biol. 2018 November 15; 443(2): 173–187. doi:10.1016/j.ydbio.2018.09.014.

Stage-specific roles of *Ezh2* and Retinoic acid signaling ensure calvarial bone lineage commitment.

James Ferguson[a], **Mahima Devarajan**[a], and **Radhika P. Atit**[b,c]

[a]Department of Biology, Case Western Reserve University, Cleveland, OH 44106.

[b]Department of Genetics and Genome Sciences, Case Western Reserve University, Cleveland OH 44106.

[c]Department of Dermatology, Case Western Reserve University, Cleveland OH 44106.

Abstract

Development of the skull bones requires the coordination of two stem progenitor populations, the cranial neural crest cells (CNCC) and head paraxial mesoderm (PM), to ensure cell fate selection and morphogenesis. The epigenetic methyltransferase, *Ezh2,* plays a role in skull bone formation, but the spatiotemporal function of *Ezh2* between the CNCC- and PM-derived bone formation *in vivo* remains undefined. Here, using a temporally-inducible conditional deletion of *Ezh2* in both the CNCC- and PM-derived cranial mesenchyme between E8.5–E9.5, we find a reduction of the CNCC-derived calvarial bones and a near complete loss of the PM-derived calvarial bones due to an arrest in calvarial bone fate commitment. In contrast, deletion of *Ezh2* after E9.5 permits PM-derived skull bone development, suggesting that *Ezh2* is required early to guide calvarial bone progenitor commitment. Furthermore, exposure to all-trans Retinoic acid at E10.0 can mimic the *Ezh2* mutant calvarial phenotype, and administration of the pan retinoic acid receptor (RAR) antagonist, BMS-453, to *Ezh2* mutants partially restores the commitment to the calvarial bone lineage and PM-derived bone development *in vivo*. Exogenous RA signaling activation in the *Ezh2* mutants leads to synergistic activation of the anti-osteogenic factors in the cranial mesenchyme *in vivo*. Thus, RA signaling and EZH2 can function in parallel to guide calvarial bone progenitor commitment by balancing the suppression of anti-osteogenic factors.

Keywords

cell fate selection; skull; mesenchyme stem cells; BMS453; incoherent feedforward loop

Corresponding author: Radhika P. Atit, Department of Biology, Case Western Reserve University, Millis Science Center, Room 316, Cleveland, OH 44106. Ph: 216.368.8819. rpa5@case.edu.

Author contributions: J.F., M.D., and R.P.A. conceived experiments, analyzed and interpreted data. J.F and R.P.A. wrote the manuscript. J.F. and M.D. carried out the experiments, and J.F. generated the figures.

Conflict of interest: The authors declare that they have no competing interests.

Introduction:

The cranial mesenchymal stem cells (CM) give rise to the bones of the head and face and originate from two different cellular origins: the cranial neural crest cells (CNCC) and the paraxial mesoderm (PM) (Jiang et al., 2002; Yoshida et al., 2008). The mammalian CNCC gives rise to the frontal, medial portion of the interparietal, temporal, and some of the facial bones. The PM primarily gives rise to the parietal, lateral portion of the interparietal, and occipital bones (Jiang et al., 2002; Yoshida et al., 2008). The calvarial bone primordia originates from a population of CM located directly above the eye in the supraorbital arch (SOA) and consists of mesenchymal stem cells from both the CNCC and PM. From E12.5 onwards, the SOA-CM expands apically over the brain, and differentiates into the frontal and parietal bones (Ishii et al., 2015; Jiang et al., 2002; Karsenty, 2008; Roybal et al., 2010; Tran et al., 2010; Yoshida et al., 2008). The calvarial bones ossify through intramembranous ossification, which is achieved through the "bone initiation program". The bone initiation program involves the sequential expression of multiple factors beginning with *Msh Homeobox 1* (*Msx1)* and *2* (*Msx2),* then *Runt-Related Transcription Factor 2* (*Runx2),* and finally *Osterix* (*Osx/Sp7*). *Msx1* and *2* expression in CM marks calvarial skeletal mesenchyme, which includes dermal and bone precursors (Han et al., 2007; Satokata and Maas, 1994; Satokata et al., 2000). *Runx2* expression leads to cell fate selection into bone progenitors, and *Osx* expression leads to a commitment of the bone progenitors to a skeletogenic fate (Karsenty and Wagner, 2002; Komori et al., 1997; Nakashima et al., 2002; Nishio et al., 2006). The developmental timing and mechanisms governing the bone initiation program and lineage restriction of the CM *in vivo* is not fully elucidated.

Multiple signaling pathways are required for the formation and differentiation of the calvarial bone *in vivo,* including Fibroblast Growth Factor (FGF), Bone Morphogenetic Protein (BMP), Wnt/β-catenin, and Retinoic Acid (RA) signaling (Ishii et al., 2015; Liu et al., 2016). For example, mutations in Wnt/β-catenin signaling lead to a loss of calvarial bone and ectopic chondrogenesis (Goodnough et al., 2012). Disruptions in various BMP and FGF signaling components can lead to numerous skull bone defects ranging from loss of structures to fused bones (Graf et al., 2016; Moosa and Wollnik, 2016; Ornitz and Marie, 2002; Pfaff et al., 2016). Among these pathways, RA signaling is a critical regulator of skull bone development. Modulation of RA signaling levels leads to an inhibition of bone growth, and it is often associated with negatively regulating targets of the Wnt, BMP, and FGF pathways. (Abe et al., 2008; Jiang et al., 2002; Kochhar et al., 1998; Lohnes et al., 1994; Maclean et al., 2009; Morkmued et al., 2017; Savory et al., 2014). The specific mechanism by which RA inhibits skull bone formation is unclear.

The Polycomb Repressive Complex 2 (PRC2) is an important epigenetic regulator in the head and face and requires RA for recruitment to specific genes (Kumar and Duester, 2014). PRC2 mediates the trimethylation of histone 3 on lysine 27 (H3K27me3) and provides positional identity of facial structures by transcriptionally poising many genes required for craniofacial development and cell fate (Lund and Van Lohuizen, 2004; Minoux et al., 2017a; Schuettengruber et al., 2017; Simon and Kingston, 2009). Mutations in the human *EZH2* gene, the catalytic component of PRC2, leads to Weaver syndrome, which is characterized by craniofacial defects including domed head and smaller mandible (Gibson et al., 2012;

Tatton-Brown et al., 2011). In mice, conditional deletion of the *Ezh2* gene in embryos leads to varying craniofacial bone defects depending on the timing and tissue of deletion, demonstrating a developmental-stage specific role for PRC2 (Dudakovic et al., 2015; Schwarz et al., 2014).

In order to understand the function of EZH2 in calvarial bone development at different developmental stages, we conditionally deleted *Ezh2* in a stage-specific manner *in vivo.* We found that *Ezh2* is required early and transiently to promote bone progenitor commitment. Inhibition of RA signaling in *Ezh2* mutants *in vivo* rescues calvarial bone development, and RA signaling activation in an E8.5-CM^{Ezh2} background leads to synergistic activation of anti-osteogenic factors. Our results suggest that RA signaling and *Ezh2* can function in parallel to balance the suppression of anti-osteogenic factors to permit later differentiation events in the calvarial bone lineage program.

Results:

Inducible deletion of *Ezh2* in cranial mesenchyme stem cells leads to stage-specific skull bone defects.

To address the stage-specific role of *Ezh2* during the CNCC- and PM-derived skull bone development, we used the tamoxifen-inducible *Pdgfra:CreER* to conditionally activate the *Rosa26Reporter (R26R)* and delete *Ezh2* in the CM prior to skull bone cell fate selection *(Pdgfra:CreER/+; R26R/+; Ezh2$^{fl/fl}$).* We initiated deletion of *Ezh2* in the CM by administering tamoxifen by oral gavage at E8.5 and E9.5 (E8.5-CM^{Ezh2}) or E9.5 and E10.5 (E9.5-CM^{Ezh2}) (Fig. 1A). *Cre*-recombination typically occurs within 24 hours after oral administration of tamoxifen. Thus, we estimate that *Ezh2* is deleted between E8.5–E9.5 in the E8.5-CM^{Ezh2} mutants and between E9.5–E10.5 in the E9.5-CM^{Ezh2} mutants. β-galactosidase lineage-marked cells were present in the majority of the CNCC-derived (plane I) and PM-derived (plane II) CM by E10.5 and E13.5 (Fig. 1B,C). Both the E8.5-CM^{Ezh2} and E9.5-CM^{Ezh2} gavage regimens were sufficient to induce extensive β-galactosidase expression in the entire cranial mesenchyme containing calvarial bone, dermal fibroblasts, and meningeal progenitors at E13.5 resulting in a dramatic reduction in H3K27me3 positive cells (Fig. S1A-C). In addition, lineage marked cells were also present throughout the facial and dentary mesenchyme. By E13.5, a whole mount phenotype was apparent in the E8.5-CM^{Ezh2} mutants in the form of a reduced mandible and frontonasal prominence leading to severe craniofacial defects by E17.5 (Fig. S2A,B).

To quantify the extent of *Ezh2* loss, we assayed for *Ezh2* mRNA and protein in E8.5-CM^{Ezh2} mutants. We obtained manually-enriched CM by removal of the ectoderm and isolation of the CM leaving the brain intact (Fig. 1D). E13.5 marks the earliest time point by which a sufficiently pure CM population can be isolated by manual dissection for subsequent analyses. Compared to E13.5 controls, we found an 80% reduction in relative amounts of *Ezh2* mRNA in E8.5-CM^{Ezh2} and 90% reduction in E9.5-CM^{Ezh2} mutants (Fig. 1E). We obtained 94% reduction in EZH2 protein in E8.5-CM^{Ezh2} mutants (n=4 from 2 litters) (Fig. 1F). To further confirm the loss of EZH2 methyltransferase function, we examined the bulk level of H3K27me3, the repressive histone modification catalyzed by

EZH2. Compared to E13.5 *Cre*-negative control CM, we found a near complete loss of bulk H3K27me3 protein in the CM of E8.5-CM^{Ezh2} mutants (n=4 from 2 litters) (Fig. 1G).

At E17.5, the E8.5-CM^{Ezh2} mutants maintained the reduced mandible and nasal region along with a domed cranium compared to controls (Fig. 1H"). In addition, E8.5-CM^{Ezh2} mutants exhibit shortened limbs, hemorrhaging of larger and smaller blood vessels, and omphalocele of the ventral body wall (Fig. S2C). In order to verify absence of embryonic lethality in our genetic cross, we calculated and obtained the expected ratio of mutants by Mendelian genetics (data not shown, n=39). These results show that E8.5-CM^{Ezh2} leads to pleiotropic effects on multiple structures and craniofacial deformities. Surprisingly, unlike the E8.5-CM^{Ezh2} mutants, the PM-derived skull bones were not lost in the E9.5-CM^{Ezh2} mutant (Fig. 1H"'). We observed ossification in the region of the parietal and occipital bone, suggesting that *Ezh2* is not required for the ossification of the PM-derived bones after E10.5. The coronal and lambdoidal suture were not readily visible in the E9.5-CM^{Ezh2} mutants; therefore, we were unable to accurately identify and quantify the area of the frontal, parietal, and interparietal bones individually. It is worth noting, the temporal bone and the tympanic ring were still disrupted in the E9.5-CM^{Ezh2} mutants (Fig. 1H). In addition, the facial bones and mandible remained truncated and the maxilla and premaxilla bones remained fused as previously observed in the E8.5-CM^{Ezh2} mutants.

Together, these phenotypes suggest a developmental stage-specific and transient role of *Ezh2* in the formation of the skull bones. Furthermore, these results imply a temporal window between E9.5–10.5 for which *Ezh2* is required to promote the formation of PM-derived skull bone formation.

E8.5-CM^{Ezh2} mutants have decreased craniofacial bone volume and size.

To further characterize the skull bone defects following loss of *Ezh2*, we performed micro-computed tomography (microCT) and morphometric analysis on the skulls of E17.5 controls and E8.5-CM^{Ezh2} mutants. Focusing our analysis on the bones of the calvaria and the dentary bones of the face at E17.5, we found malformations and truncations in most of the -craniofacial bones with a 65% decrease in overall relative bone volume in the mutants (control: 1.0+0.09, mutant: 0.36+0.11; n=3 controls, 4 mutants) (Fig. 2A-C).

To quantify the craniofacial bone deformities in more detail, we used the recently described embryonic craniofacial bones landmarks (Ho et al., 2015). The facial bones such as the mandible, maxilla, pre-maxilla, and nasal bones were present, but their morphology was compromised (Fig. 2B, Fig. S3A,B). Relative to the control, the overall length of the mandible (mm) from the most posterior point of the condylar process to the most anterior point of the mandible was decreased by 60% (control: 1.0+0.11, mutant: 0.42+0.05 $p=0.04$), and bone volume (mm^3) was reduced by 83% (control: 1.0+0.04, mutant: 0.17+0.12; n=3 controls, 4 mutants) (Fig. S3A). The combined relative length of maxilla and premaxilla from the posterior-medial point of the palatine process of the maxilla to the most distal point was decreased by 28% in the mutant (control: 1.04+0.08, mutant: 0.74+0.09; p=0.04). The combined relative volume of the nasal, premaxilla and maxilla region was reduced by 42% in the E8.5-CM^{Ezh2} mutant (control: 1.0 +0.28, mutant: 0.61+0.11; n=3 controls, 4 mutants) (Fig. S3B). It is worth noting, we could not clearly identify a separate maxilla and

premaxilla bone, and it was unclear whether the premaxilla was missing or if it was fused with the maxilla.

Interestingly, in the calvaria, the some of the CNCC- and most of the PM-derived bones were differentially reduced, indicating variable sensitivity to the deletion of *Ezh2.* The morphology of the CNCC-derived frontal bone was compromised, and the relative volume was diminished by 39% (control: 0.94+0.43, mutant:0.57+0.17; n=3 controls, 4 mutants). In contrast, the PM-derived parietal bone relative volume was decreased by 85% (control: 1.2+0.33, mutant: 0.16+0.14; n= 3 controls, 4 mutants) and the PM-derived occipital bone was nearly absent in the mutant (Fig. 2B,D). The interparietal bone, which has contributions from both the CNCC and PM, has similar morphology between the controls and mutants, but the relative volume was decreased by 45% in the mutant (control: 1.1+0.66, mutant: 0.61+0.30; n=3 controls, 4 mutants) (Fig. 2D, Fig. S3C). In addition, CNCC-derived temporal bone, inner ear bones, and the tympanic ring were absent in the E8.5-CM^{Ezh2} and E9.5-CM^{Ezh2} (Fig. 2B, 1H). These results demonstrate a sensitivity of the posterior structures, primarily PM-derived, to *Ezh2* expression between E9.5 and E10.5.

To further analyze the morphology of the CNCC-derived frontal bone and interparietal bone, we performed morphometric measurements to quantify changes in the relative dimensions of the frontal and interparietal bones (Fig. 2B,E). Relative to the controls, both the length (mm) and height (mm) of the frontal bone were reduced by roughly 25% (length: control: 1.0+0.06, mutant: 0.76+0.10; p=0.0005; height: control: 1.1+0.16, mutant: 0.79+0.2; p=0.03) in the E8.5-CM^{Ezh2} mutants. In addition, the distance (width) between the most posterior-superior points of the left and right frontal bones was increased by 1.5 fold (control: 0.97+0.12, mutant: 1.5+0.08; p=0.04) in the mutants indicating a larger fontanelle. The interparietal bone, despite a decrease in overall volume (Fig. 2D), did not exhibit major changes in morphology with a 4% decrease in relative length in the mutant compared to the control (control: 0.99+0.09, mutant: 0.96+0.05; p=n.s.) (Fig. 2E).

Varying levels of deformities in the mandible, the snout region, and the calvarial bones in the E8.5-CM^{Ezh2} mutant demonstrates the differential effect of *Ezh2* deletion in bone formation of different tissue origins. Considering the anterior skull is CNCC-derived and the interparietal bone has contributions from both the CNCC and PM, the greater disruption of the purely PM-derived parietal and occipital bones indicates a sensitivity of the PM to the deletion of *Ezh2.*

Cell survival and proliferation is not dramatically altered in E8.5-CM^{Ezh2} mutants at E10.5.

Conditional mutants lacking *Ezh2* exhibit an overall decrease in bone size and volume in late fetal stages. To examine changes in cell survival and proliferation, we quantified changes in active Caspase-3 and EdU in E8.5-CM^{Ezh2} mutants. At E10.5, quantification of the cells positive for activated Caspase-3 in the CM revealed a modest 2.6% significant increase in plane I (frontal bone primordia) only and comparable numbers to control in plane II (parietal bone primordia) in E8.5-CM^{Ezh2} mutants without significant changes in total cell number in all the examined regions (n=5 controls and 6–8 mutants, 2 litters) (Fig. S4A,B,D). In the frontonasal process, quantification of activated Caspase-3 positive cells showed a more dramatic 8% increase in E8.5-CM^{Ezh2} mutants which could account for the facial bone

defects (n=5–7) (Fig. S4E). The cell proliferation index at E10.5, as detected by 5-ethynyl-2´-deoxyuridine (EdU) incorporation, was comparable in all regions (n=5–7, 2–3 litters) (Fig. S4C-E). Additionally, we did not find significant changes in cell survival, proliferation, and total cell number in the CM and in the frontonasal mass at E11.5 and E13.5 (data not shown). In the E9.5-CM^{Ezh2} mutants at E11.5, the total number of cells expressing activated Casapse-3 revealed a 2.6% significant increase in plane I and was comparable in plane II (Fig S4F). Considering both E8.5-CM^{Ezh2} and E9.5-CM^{Ezh2} exhibit small changes in cell survival in the frontal and parietal bone primordia roughly 24 hours after deletion of *Ezh2*, we deduce that changes in cell survival and proliferation do not fully account for the loss of the parietal bone in the E8.5-CM^{Ezh2} mutants. These results indicate that the loss of calvarial bones is not due to changes in cell survival and proliferation, and that the mechanism by which *Ezh2* regulates skull bone formation may differ between individual bones or structures.

E8.5-CM^{Ezh2} mutants exhibit defects in the differentiation of the calvarial bone progenitors.

To further investigate the role of *Ezh2* in regulating bone formation in the CM, we next wanted to determine if the defects in the frontal and parietal bones in the E8.5-CM^{Ezh2} mutants result from an arrest in cell fate selection and commitment. Therefore, we examined the expression of genes in the calvarial bone initiation program, which consists of the expression of MSX1/2, RUNX2, and OSX, in the frontal (plane I) and parietal bone (plane II) primordia (n=3–5, from 2 litters) (Fig. 3A) (Karsenty, 2008; Roybal 2010). At E11.5, the cranial mesenchyme marker MSX1/2 which is required for cranial bone had comparable expression domains in both plane I and plane II with a similar number of cells expressing MSX1/2 between controls and E8.5-CM^{Ezh2} mutants (Fig. 3B) (Roybal 2010). At E13.5, the morphology of the RUNX2 domain was shifted ventrally in the frontal bone and less compacted in the parietal bone primordia in the E8.5-CM^{Ezh2} mutants. RUNX2 expression is first step in lineage selection and the establishment of bone progenitors (Karsenty, 2008; Komori et al., 1997). The number of RUNX2 positive cells in plane I and plane II was slightly diminished in the mutants but did not approach statistical significance (Fig. 3C). In addition, the expression domain of bone progenitor markers, alkaline phosphatase (AP), was comparable in both plane I and plane II in the controls and E8.5-CM^{Ezh2} mutants (S5A). These results suggest the disruption in bone formation in E8.5-CM^{Ezh2} mutants was not due to failure to establish the bone progenitors. Next, we examined the expression domain of OSX protein, which is downstream of RUNX2, and is required for cell fate commitment of the bone progenitors to osteoblasts (Karsenty, 2008; Nakashima et al., 2002). In the E8.5-CM^{Ezh2} mutants at E13.5, we found that the OSX-positive expression domain and the number of OSX positive cells were diminished in plane I and nearly absent in plane II (Fig. 3D). In comparison to the E8.5-CM^{Ezh2} mutants, the E9.5-CM^{Ezh2} mutants do not show a noticeable disruption in the establishment of the AP and OSX-positive domains (Fig. S5B and data not shown). Our studies show that *Ezh2* is not required for the early specification of the bone progenitors, but for the establishment of OSX positive osteoblasts. In addition, these results further refine the previous models describing the role of EZH2 in skull bone development by identifying a defined developmental window in which *Ezh2* is required (Dudakovic et al., 2015; Ferguson et al., 2017; Schwarz et al., 2014).

Retinoic acid inhibits skull bone formation and is required for *Ezh2* expression in the cranial mesenchyme

Since *Ezh2* is required between E9.5 and E10.5 for the expression of OSX at E13.5, we next sought to determine if intermediate signaling factors are required for the regulation of the frontal and parietal bones by *Ezh2.* We queried the literature and found that administration of all-trans RA (at-RA) at E10.0 leads to craniofacial defects strikingly similar to the E8.5-CM^{Ezh2} mutants (Jiang et al., 2002). In addition, mice lacking *Cyp26b1*, which is required for breakdown of RA, leads to a severe reduction in the skull bones (Maclean et al., 2009). To examine the effects of RA signaling on *Ezh2* transcription and E8.5-CM^{Ezh2} phenotype, we took a pharmacological approach to generate conditions of increased RA-signaling *in vivo*. Consistent with previous studies, administration of all-trans retinoic acid (at-RA) by oral gavage at E10.0 to *Cre*- control mice resulted in a reduction in the skull bones (Fig. 4A). In E13.5 CM, relative mRNA expression level of *HoxA1,* a positively regulated transcriptional target of RA signaling, was upregulated nearly 10 fold after oral gavage of at-RA, demonstrating increased activation of RA-signaling (Williams et al., 2005) (Fig. 4B). We found the relative mRNA levels of *Ezh2* were upregulated by 5 fold in response to at-RA exposure. Relative to the other PRC2 components, changes in expression levels were specific to *Ezh2,* as the expression levels of *Suz12* and *Eed* exhibited a modest or no change respectively following administration of at-RA (Fig. 4C). At E17.5, we found reduced area of mineralized frontal and parietal bones. Quantification of the total area of each bone revealed a 60% decrease in the frontal bone and 80% decrease in the parietal bone in the at-RA treated embryos relative to untreated controls. In addition, the facial bones were truncated and the embryos were overall smaller (Fig. 4D; S6A).

We next examined any changes in cell fate commitment following administration of at-RA. Noting that sufficient *Cre*-recombination in the E8.5-CM^{Ezh2} mutants occurs around E9.5, we next administered at-RA by oral gavage to *Cre*- controls at E9.5. Administration of at-RA at E9.5 resulted in higher protein expression by immunofluorescence of the RA-sensitive gene, Retinoic Acid Receptor Gamma (RARγ), demonstrating increased RA-signaling in the CM (Fig. 4E) (Balmer and Blomhoff, 2002). Similar to the E8.5-CM^{Ezh2} mutants, administration of at-RA lead to a reduction in OSX expression in the parietal bone (Fig. 4F). This is noteworthy as the disruption of OSX expression is similar E8.5-CM^{Ezh2} mutants, but occurs in samples with increased *Ezh2* mRNA levels (Fig4C). Together, these results demonstrate excess RA signaling at E9.5 and 10.0 can mimic the E8.5-CM^{Ezh2} mutant phenotypes, allowing us to test the hypothesis that RA signaling positively regulates and EZH2 negatively regulates the expression of anti-osteogenic factors to promote skull bone formation in a incoherent type-1 feedforward model (I1-FFL) where two arms act in opposition (Alon U, 2007)(Fig. 4G).

In vivo inhibition of retinoic acid signaling partially restores skull bones.

To generate a loss of RA-signaling model, we used a small molecule inhibitor to neutralize RA-signaling at the receptor level. Because RAR-γ is the most abundantly expressed RAR in the CM, and is unaffected by deletion of *Ezh2* (n=4), we administered the small molecule inhibitor, BMS-453, by oral gavage to E8.5-CM^{Ezh2} mutants (Fig. 5A; S6B). BMS-453 is an efficient bioavailable antagonist of Retinoic Acid Receptor Alpha (RAR-α) and RAR-γ *in*

vivo with a higher affinity to RAR-γ (Chen et al., 1995; Chung et al., 2011; Matt et al., 2003). At E13.5, in manually enriched CM following administration of BMS-453, we found a dose-dependent decrease in the mRNA levels of the RA signaling target gene, *Cellular retinoic acid binding protein2* (*Crabp2),* in both controls and E8.5-CM^{Ezh2} mutants (n=3–5 from two litters) (Fig. S6C) (Williams et al., 2005). At the 3.5μg/g body weight dosing regimen of BMS-453, the relative level of *Crapb2* mRNA was diminished by 50% without prominent drug induced defects as seen with 5μg/g body weight dose (Compare Fig. S6D with S2B). In agreement with the up regulation of *Ezh2* expression levels following at-RA treatment (Fig. 4C), administration of 3.5μg/g BMS-453 resulted in a 70% decrease in *Ezh2* expression levels in E13.5 manually isolated CM (Fig. 5B). At E17.5, administration of 3.5μg/g BMS-453 treated E8.5-CM^{Ezh2} mutants revealed a partial rescue of the parietal and occipital bone relative to untreated E8.5-CM^{Ezh2} mutants (n=9 from two litters) (Fig. 5C compared to Fig. 1H). Quantification of the relative area of alizarin red stained bone also confirmed the recovery of the parietal bone (Fig. 5D, n=9). We also observed improvement in the extension of the mandible and maxilla bones and partial recovery of the inner ear bones in some treated mutants. In the three E17.5 litters analyzed, the E8.5-CM^{Ezh2} mutants showed a range of rescue of parietal and occipital bone in E8.5-CM^{Ezh2} mutants (Fig. 5C’’, C’’’). In addition, the quantification revealed a small, but statistically significant, decrease in area of the frontal bone of the E8.5-CM^{Ezh2} mutant embryos treated with BMS-453.

To determine if BMS-453 treatment restored differentiation of the bone progenitors at E13.5, we examined OSX expression in the parietal bone primordia. Compared to untreated E8.5-CM^{Ezh2} mutants, which lack OSX expression in the parietal bone primordia (Fig. 3D), E8.5-CM^{Ezh2} mutants treated with BMS-453 showed a partial restoration of OSX expression, (Fig. 5E, n=6). The restoration of the posterior PM-derived calvaria bone formation in E8.5-CM^{Ezh2} by RA signaling inhibition, indicate that simultaneous inhibition of the positive and negative arms of I1-FFL is able to partially rescue Osx expression and posterior calvarial bone formation (Fig. 5F). Together, these results demonstrate that tight control of RA-signaling levels is required to ensure skull bone formation, and that *Ezh2* transcription is sensitive to RA-signaling.

Deletion of *Ezh2* or activation of RA-signaling leads to the up regulation of anti-osteogenic factors.

To identify anti-osteogenic factors regulated by EZH2 and RA, we took a candidate approach to identify changes in gene expression in E8.5-CM^{Ezh2} mutants. (Balmer and Blomhoff, 2002; Creuzet et al., 2002; Hunt et al., 1991; Krumlauf, 1994; Lee et al., 2014; Savory et al., 2014) (Bracken et al., 2006; Mirzamohammadi et al., 2016; Schwarz et al., 2014). In E13.5 manually enriched CM of E8.5-CM^{Ezh2} mutants (Fig. S7A), we did not find significant changes in mRNA levels of *Sprouty2, Serpine1, Id1,* or *Axin2* which are readouts for FGF, TGF-β, BMP, and Wnt signaling pathways, respectively (n=3–8 from two litters) (Fig. S7B). In addition, we did not see changes in the expression of RA signaling pathway components, such as *Rar-γ*, *Stra6*, and *Crabp2*, between controls and E8.5-CM^{Ezh2} mutants at 13.5, suggesting the RA pathway components are not altered in the absence of *Ezh2* (Fig. S6B; S7C) (Table S1) (Balmer and Blomhoff, 2002). Surprisingly, of all the other candidate genes queried, only a subset exhibited considerable increase (>10 fold). These include the

following: the regional identity *Hox* genes, the cell cycle regulator, *Cyclin-dependent kinase Inhibitor 2a (Cdkn2a)*, and Hedgehog signaling regulator and positional identity gene, *Heart and neural crest derivatives expressed 2* (*Hand2)* (Table S1). Among the *Hox* genes queried, we identified *HoxA1* and *HoxC8* as the most upregulated *Hox* genes with a ~250-fold and 6–12-fold increase in mRNA levels, respectively (Fig. 6A. S7D) (Table S1) (Dudakovic et al., 2015; Minoux et al., 2017a; Schwarz et al., 2014). *Cdkn2a* is a known cell cycle regulator, and due to no significant changes in cell proliferation in the CM in E8.5-CM^{Ezh2} mutants, we focused on the *Hox* genes and *Hand2.* Both the *Hox* genes and *Hand2* have been shown to be positively regulated by RA and inhibit osteogenesis, highlighting them as potential anti-osteogenic factors responsible for the disruption in the skull bone in the E8.5-CM^{Ezh2} mutants (Fig6A) (Balmer and Blomhoff, 2002; Carroll and Capecchi, 2015; Firulli et al., 2005; Funato et al., 2009; Krumlauf, 1994; Lee et al., 2014).

To test if the up regulation of *Hox* genes and *Hand2* following deletion of *Ezh2* works independently or synergistically with RA-signaling activation in this context, we administered 100ug/gm body weight of exogenous at-RA to pregnant females carrying wild-type, Cre-control embryos, or E8.5-CM^{Ezh2} at 10.0 (Jiang et al., 2002). At-RA exposure led to significant up regulation of *HoxA1, HoxC8,* and *Hand2,* but at lower levels than E8.5-CM^{Ezh2} mutants. Importantly, administration of at-RA to E8.5-CM^{Ezh2} mutants consistently compounded the increase of *HoxA1, HoxC8,* and *Hand2*, mRNA levels (Fig. 6A).

To further demonstrate that these anti-osteogenic factors were direct targets of PRC2 in the CM, we analyzed the H3K27me3 enrichment on *HoxA1, HoxC8,* and *Hand2* from our previously published H3K27me3 chromatin immunoprecipitation followed by DNA sequencing (ChIP-seq) dataset (GSE96872) (Ferguson et al., 2017). In E13.5 control CM, the *HoxA* and *HoxC* clusters, and *Hand2* genes had a blanket H3K27me3 modification across the entire loci in E13.5 cranial mesenchyme (Fig. 6B), indicating they are directly regulated by PRC2. Furthermore, the *Osx* locus had minimal enrichment of H3K27me3 further supporting the hypothesis that changes in OSX expression in the E8.5-CM^{Ezh2} mutants is due to an indirect mechanism. These results suggest that EZH2 indirectly affects OSX expression. These results also show that RA-signaling and EZH2 can work in parallel to synergistically regulate the expression of specific anti-osteogenic factors *in vivo* (Balmer and Blomhoff, 2002; Carroll and Capecchi, 2015; Krumlauf, 1994; Lee et al., 2014).

In order to decipher the putative mechanism of the rescued mutants, we tested if ectopic *HoxC8* gene expression in E8.5-CM^{Ezh2} mutants was attenuated in the rescued BMS-453-treated E8.5-CM^{Ezh2} mutants. As expected, at E13.5, HOXC8 protein expression was below the levels of detection in untreated and BMS-453-treated control embryos in the region of parietal bone primordia (Fig. 6C'). In contrast, we detected ectopic HOXC8^{+} cells in the region of parietal bone primordia E8.5-CM^{Ezh2} and in the facial mesenchyme. (Fig. 6C'' n=4, data not shown). In a comparable region, we observed a qualitatively diminished number of HOXC8^{+} cells in the rescued BMS-453-treated E8.5-CM^{Ezh2} mutants (Fig. 6C''', n=3). These results indicate that RA signaling inhibition can lead to decreased expression of the anti-osteogenic factor, *HoxC8,* in the E8.5-CM^{Ezh2} mutants and may contribute to rescuing calvarial bone development.

Taken together, these data suggest that EZH2 and RA-signaling must maintain strict balance in activity to synergistically regulate anti-osteogenic factors in order to allow for the commitment to the calvarial bone lineage. Thus, the overlapping phenotypes of E8.5-CM^{Ezh2} mutants and RA pathway mutants suggest they share similar functions in calvarial bone formation allowing us to build a proposed hypothetical model by which *Ezh2* promotes skull bone formation (Fig. 6D).

Discussion:

In this study, we examined the basis of the anti-osteogenic effects of *Ezh2* deletion and RA signaling activation during calvarial bone differentiation. We found a stage-specific requirement of *Ezh2* for OSX expression and directing osteoblast fate commitment in the calvaria. Considering OSX is required for intramembranous ossification in the skull and in the periosteum of long bones, our results highlight a specific role of *Ezh2* in intramembranous ossification (Nakashima et al., 2002). We show a restoration of PM-derived skull bones in *Ezh2* mutants by inhibiting RA signaling, demonstrating that EZH2 functions to repress anti-osteogenic factors that are poised to be regulated by RA signaling in an incoherent feedforward loop. The critical timing of repression ensures commitment and differentiation of calvarial bone progenitors. We discuss the implications of our findings in more detail below.

The transient role of *Ezh2* in impacting the lineage-commitment of calvarial bone progenitors.

The distinct phenotypes at different developmental stages in conditional *Ezh2* mutants reveal a developmental stage-specific role of *Ezh2* in skull bone formation. Three plausible explanations of this effect are: First, the posterior skull bones develop at a later developmental-stage than the anterior bones. In the SOA, *Msx1* and *2* can first be detected in the frontal bone primordia at E10.5 with ossification at E14.0. In comparison, in the parietal bone region, expression of *Msx2* only can first be detected in the parietal bone primordia at E11.5 with ossification at E14.5 (Han et al., 2007). Other published conditional mouse *Ezh2* mutants support its developmental-stage specific role in impacting the calvarial bone lineage. Loss of *Ezh2* in pre-migratory CNCC prior to E8.5 using *Wnt1Cre* leads to a near complete loss of the CNCC-derived facial and frontal bones (Schwarz et al., 2014). In contrast, loss of *Ezh2* in the CNCC and PM from E9.5 using *Dermo1Cre* does not lead to depletion of H3K27me3 modification and loss of the CNCC and PM-derived bones (Ferguson et al., 2017).

The second possibility is that the anti-osteogenic factors exhibit varying levels of sensitivity to RA-signaling. *In vitro*, different genes have been demonstrated to have different levels of sensitivity to RA-signaling (Balmer and Blomhoff, 2002; Williams et al., 2005). It is possible the anti-osteogenic are sufficiently up-regulated after the establishment of the bone progenitors and *Runx2* expression. As a result, we do not observe changes in the bone initiation program until the OSX expression is disrupted in the CM. Thus, deletion of *Ezh2* prior to E10.5 is required to enable sufficient up-regulation of the anti-osteogenic factors. Alternatively, our result does not rule out the distant possibility of a temporal lag in

depletion of H3K27me3 modifications and dysregulation of anti-osteogenic factors after the onset of RUNX2 expression. However, the acute changes in cell survival of the frontonasal process mesenchyme at E10.5 in the E8.5-CM^{Ezh2} mutants suggest rapid changes in gene expression following deletion of *Ezh2.*

A third possibility is that lineage selection of calvarial bone precursors in the CM occurs prior to lineage-specific marker expression. By comparing E8.5-CM^{Ezh2} and E9.5-CM^{Ezh2} mutants, the critical window of lineage-selection of parietal bone progenitors would occur between E9.5 and E10.5, prior to *Msx2* expression at E11.5 in the parietal bone primordia. The restricted timing of RA signaling activation and rescue lends evidence to support to this critical temporal window. The concept of lineage selection and restriction before lineage-specific marker expression has also been observed in the premigratory trunk NC in multiple organisms (Dorsky et al., 2000; Krispin et al., 2010; Schilling and Kimmel, 1994). Additional genetic studies with temporally-induced clonal lineage analysis will be required to demonstrate if *Ezh2* functions in lineage selection and restriction in the CM before the onset of *Msx1* and *2*.

Taken together, our results with temporally inducible conditional deletions of *Ezh2* reveal a defined temporal window for the commitment to the calvarial bone lineage and further refines the previous model of *Ezh2* in craniofacial bone differentiation (Schwarz et al., 2014).

Loss of *Ezh2* and increased in RA-signaling synergistically promotes expression of anti-osteogenic factors in the CM in an incoherent feedforward loop.

Previous studies have demonstrated a wide range of craniofacial phenotypes that result from positive and negative modulation of RA signaling. *RARα;RARγ* compound null mouse mutants have a range of phenotypes from exencephaly to underdeveloped skull bones (Lohnes et al., 1994). Loss of *Cyp26B1*, a retinoic acid catabolic enzyme, results in truncation of facial and frontal bones and a lack of ossification of the parietal and interparietal bones at E17.5 (Maclean et al., 2009). In our study, at-RA exposure at E10.0 led to a more diminished parietal than frontal bone, which is consistent with previous RA signaling gain of function studies (Jiang et al., 2002; Maclean et al., 2009).

RA signaling activation in the E8.5-CM^{Ezh2} mutant background leads to a compounded increase in target genes with known anti-osteogenic function; thereby, indicating that RA signaling activation and *Ezh2* have opposing functions in calvarial bone formation. Interestingly, we also found that activation of RA-signaling increases *Ezh2* mRNA expression levels. These results indicate that a balance of RA-signaling and *Ezh2* expression is required to maintain skull bone lineage commitment. In agreement with this hypothesis, RA has been shown to recruit PRC2 components and H3K27me3 modification to a Retinoic Acid Responsive Element (RARE) near the promoter of *Fgf8* and *HoxB1* leading to transcriptional repression (Kumar and Duester, 2014). The binding of RA to a RARE element can mediate transcriptional repression by recruiting PRC2 to specific genes (Kumar and Duester, 2014). In the context of the CM, RA signaling can function with EZH2 in an I1-FFL, where the two arms of the loop can function in opposition (Alon, 2007). In one arm, RA recruits PRC2 to anti-osteogenic factors, resulting in H3K27me3 enrichment and

transcriptional repression. In the absence of EZH2, RA can function as a transcriptional activator and induce the expression of anti-osteogenic factors on the other arm. Particularly, I1FFL can generate a pulse effect which can be used to explain the transient and stage-specific role of RA signaling and EZH2 in the commitment of calvarial bone progenitors (Basu et al., 2006). Additional genetic studies with RAR mutants and chromatin immunoprecipitation of CM will be required to tease apart the epistatic and mechanistic relationships between these two major regulators.

The exact mechanism by which RAR antagonism partially rescues E8.5-CM^{Ezh2} mutants is unclear and our results offer clues. We detected substantial increase in a class of known targets genes which appear to be poised to respond dramatically to exogenous RA signaling in the CM, such as *HoxA1, HoxC8,* and *Hand2,* in E8.5-CM^{Ezh2} mutants (Balmer and Blomhoff, 2002; Williams et al., 2005; Zhao et al., 2009). Our data suggest RAR signaling inhibition in the E8.5-CM^{Ezh2} mutant can decrease the ectopic expression of well-characterized anti-osteogenic factors such as *HoxC8*. Additional studies with RARE reporters and Mass-spectroscopy will be required to visualize and quantify the changes in RA signaling in the CM.

In order to determine the anti-osteogenic role of *HoxA1, HoxC8,* and *Hand2,* future studies using functional mouse genetics and gene expression profiling in CNCC- and PM-specific CM of E8.5-CM^{Ezh2} mutants are required. The *Hox* genes are a well-established target of PRC2 mediated transcriptional repression in multiple cell types *in vitro* and in the CM *in vivo* (Dudakovic et al., 2015; Ferguson et al., 2017; Minoux et al., 2017b; Schwarz et al., 2014). In addition, numerous *Hox* genes are well known targets of RA-signaling (http://www.uniprot.org/uniprot/Q15910) (Balmer and Blomhoff, 2002; Krumlauf, 1994). In our E8.5-CM^{Ezh2} mutants, we identified an up regulation of multiple *Hox* genes in the E13.5 CM, which is *Hox*-negative in controls. It is possible that the ectopic expression of a specific *Hox* gene or multiple *Hox* genes may lead to a change in regional identity and results in the loss of skull bones. Out of the *Hox* genes queried, *HoxC8 w*as the most significantly increased *Hox* gene which may have an anti-osteogenic function in calvarial bone. *In vivo*, conditional misexpression of *HoxC8* in the head and face CM leads to a near complete loss of skull bones and a truncation of the face resembling our E8.5-CM^{Ezh2} mutants (Carroll and Capecchi, 2015). We also observed attenuated expression of HOXC8 protein expression in the CM of the parietal bone region following inhibition of RA signaling. Future studies that genetically alter *HoxC8* gene dosage in E8.5-CM^{Ezh2} mutants would be required to demonstrate that up regulation of a single, regionally expressed *Hox* gene mediates the phenotype in E8.5-CM^{Ezh2} mutants. Follow up biochemical and proteomic studies will also be required to reveal the anti-osteogenic mechanism of HOXC8. Alternatively, the combinatorial effect of the ectopic expression of multiple *Hox* genes could lead to the bone defects observed in our E8.5-CM^{Ezh2} mutants. In addition to *HoxC8,* we also observed an up regulation of multiple other *Hox* genes that could negatively affect skull bone development in our E8.5-CM^{Ezh2} mutants. For example, *HoxA1* $^{-/-}$ mutants have craniofacial defects and *HoxA1* transcription is responsive to retinoic acid in CM (Fig. S7) (Balmer and Blomhoff, 2002; Boylan et al., 1993; Boylan et al., 1995). In zebrafish, *HoxA1* overexpression or exogenous administration of at-RA leads to an identity switch of the first branchial arch (Alexandre et al., 1996; Hill et al., 1995). It is worth noting, *HoxA2,* the *Hox* gene often

associated with bone inhibition, was not significantly upregulated in our E8.5-CM^{Ezh2} mutants (Fig. S7) (Grammatopoulos et al., 2000; Trainor and Krumlauf, 2001).

HAND2 is a basic helix-loop-helix transcription factor that may function as a negative regulator of intramembranous bone formation. HAND2 protein has been shown to directly bind to RUNX2 protein and prevent its transactivation function (Funato et al., 2009). *Hand2* transcription is positively regulated by teratogenic doses of RA signaling, and HAND2 protein can function as an upstream regulator of Hedgehog signaling which can negatively regulate bone (Abzhanov et al., 2007; Charité et al., 2000; Galli et al., 2010; Zhao et al., 2009). Thus, future studies focusing on reducing the dosage of *Hand2* in our E8.5-CM^{Ezh2} mutants will be required to demonstrate if HAND2 is a key component of an anti-osteogenic network that is repressed by EZH2 during intramembranous bone differentiation. Along with the *Hox* genes and *Hand2*, the dysregulation of additional unidentified anti-osteogenic factors could result in a loss of skull bones in the *Ezh2* mutants. A systematic effort will be required to identify new anti-osteogenic targets of *Ezh2* in CNCC- and PM-derived CM using developmental stage-specific mutants with new inducible lineage-specific genetic tools.

In this study, we show that stage-specific conditional loss of *Ezh2* in the CM can be neutralized by small molecule antagonism of RAR, providing evidence that EZH2 in the CM is required for repressing the expression of anti-osteogenic factors that are poised to respond to RA signaling in a I1FFL. Our data provide new insights into the dynamic formation of calvarial bones highlighting the spatial and temporal differences in successful progression of osteogenesis during intramembranous bone formation.

Methods:

Mice:

Pdgfra-CreER (JAX stock #018280) (Rivers et al., 2008), *Rosa26 Reporter* (AX stock #003309) (Soriano,1999), and *Ezh2 floxed* (*Ezh2*^{fl}) (JAX stock #022616) (Shen et al., 2008). For timed matings, *Pdgfra-CreER;Ezh2*$^{fl/fl}$ males were crossed with *R26R/R26R;Ezh2*$^{fl/fl}$ females overnight. Mice were checked for vaginal plugs and then separated in the morning. Vaginal plug day was assigned as embryonic (E) 0.5. *CreER* recombination was induced by oral gavage at 25ug Tamoxifen/g body weight (BW) (Sigma T5648) to pregnant dams. Tamoxifen was dissolved in corn oil and administered at 5 p.m. of the designated day. For each experiment, a minimum of five mutants with litter-matched Cre negative controls from two to three litters were studied unless otherwise noted. Case Western Reserve University Institutional Animal Care and Use Committee approved all animal procedures in accordance with AVMA guidelines (Protocol 2013–0156, Animal Welfare Assurance No. A3145–01).

Histology, β-Galactosidase, and Immunohistochemistry:

Heads of E10.5–13.5 embryos were drop-fixed in 4% paraformaldehyde (PFA) for 20–35 min, respectively, at 4^{0}C and cryopreserved as previously described (Atit et al., 2006). Embryos were cryosectioned at 10 microns in the coronal plane in the frontal and parietal

bone primordia. β-galactosidase staining on cryosections was performed as previously described (Rivera-Perez et al., 1999).

For immunofluorescence on cryosections, sections were dried at room temperature, washed in 1x PBS and blocked in goat serum or donkey serum. For mouse raised antibodies, block buffer from the Vector M.O.M Kit (BMK-2202) was used. Primary antibodies were incubated overnight at 4°C, washed next day in 1x PBS, incubated with species- specific secondary antibody (below) for one hour at room temperature, and then washed with DAPI 0.5μg/mL, and mounted with Fluoroshield (Sigma F6057).

For immunofluorescence, the following primary antibodies were used: rabbit anti-H3K27me3 (1:1000; Cell Signaling 9733, Antibody registry: AB_26160629), Rabbit anti-Caspase3 (1:250; Abcam13847, Antibody registry: AB_443014), Rabbit anti-OSX (1:1000 Abcam ab94744, Antibody registry: AB_10674971), mouse anti-MSX1/2 (DSHB 4G1, Antibody registry: AB_531788), goat anti-RUNX2 (1:250 R&D AF2006, Antibody registry: AB_2184528) rabbit anti-HOXC8 (1:500, Abcam ab86236, Antibody registry: AB_1925078), rabbit anti-RARG (1:1000, Cell Signaling D3A4, Antibody registry: AB_10998934). Appropriate species-specific Alexafluor secondary antibodies were used (1:500; Invitrogen). Images were captured using the Olympus BX60 microscope and Olympus DP70 digital camera using DC controller software. Confocal images were captured on the Leica TCS SP8 (Leica Biosystems) using Application Suite X software (Leica Biosystems). Images were processed in Adobe Photoshop and Fiji/ImageJ (Schindelin et al., 2012; Schneider et al., 2012).

For alkaline phosphatase staining, sections were then washed in PBS-T (0.1% Tween-20 in PBS) for 10 minutes, then TBS-T (0.1% Tween-20 in TBS) for 10 minutes, then washed in NTMT (100mM Tris, pH 9.4, 100mM NaCl, 60mM $NgCl_2$, and 0.02% Tween-20) for 10 minutes. Embryos were stained 20μl/mL NBT/BCIP (Roche 11681451001) in the dark for 20 min. at RT. Slides were then washed in PBS and mounted with aqueous mounting medium.

RT-qPCR:

At E13.5, the supraorbital cranial mesenchyme was isolated by manual dissection. Following manual removal of the ectoderm, an incision was made around the circumference of the neurocranium, and the tissue covering the brain was manually disassociated. The CM isolated consists of the neural crest and mesoderm derived cranial mesenchyme. RNA was isolated as previously described (Hamburg-Shields et al., 2015). Relative mRNA expression was quantified using 5 ng of cDNA on a StepOne Plus Real-Time PCR System (Life Technologies) and the ΔΔCT method (Schmittgen and Livak, 2008). Commercially available TaqMan probes (Life Technologies) specific to each gene were used (Table S1). CT values were normalized to *β-actin* (Invitrogen 4352663). ΔΔCT values were obtained by normalizing the ΔCT values to the average ΔCT values of the controls. Relative mRNA fold change was determined using the ΔΔCT values.

Protein Isolation and immunoblotting

E13.5 cranial mesenchyme was enriched and collected by manual dissection as described above. Protein was isolated using RIPA buffer. Proteins were separated by SDS-PAGE using Mini-PROTEAN TGC gels (BioRad #456–1084). Western Blots were performed with the following primary antibodies: rabbit anti-H3K27me3 (1:1000, Cell Signaling 9733) and rabbit anti-EZH2 (1:500, Cell Signaling #5246). Species-specific HRP-conjugated secondary antibodies were used at 1:10,000. Immunoblots were probed with anti-β-TUBULIN (1:400, Santa Cruz 9104) as a loading control. Protein was detected using an Amersham ECL Western Blotting Analysis System (GE Healthcare RPN2109), and imaged using an Odyssey FC Imaging System (Li-Cor). Relative protein levels were quantified using Image J/ Fiji.

MicroCT:

E17.5 heads were fixed and stored in 95% ethanol for at least 24 hours. Heads were then re-hydrated overnight in PBS for 24 hours prior to imaging. MicroCT images were acquired using a Bruker SkyScan1172 (Bruker MicroCT, Kontich, Belgium) with an 11 MPix camera at an isotropic voxel size of 20 μm^3 employing an 0.5mm-thick aluminum filter. An applied x-ray tube voltage of 50 kV with an x-ray intensity of 100 μA was applied over 180 degrees of rotation with acquisition every 0.7 degrees. Camera pixel binning of 4×4 was applied. Reconstruction was carried out with a modified Feldkamp algorithm using the SkyScan NRecon software (Feldkamp et al., 1984; Yan et al., 2008). Ring artifact reduction of 5 and beam hardening correction of 10 were applied. MicroCT 3D images were visualized using CTvox (BrukerMicroCT). Images were pseudo-colored in Adobe Photoshop. Quantification was performed using Amira 6.01 (Thermo Fisher Scientific) using the “Materials Statistics” tool.

Whole mount skeletal preparation:

All steps were performed at room temperature. Embryos were fixed in 95 % ethanol overnight. Samples were then placed in acetone overnight. Embryos were then placed in alcian blue (Sigma A5268) dissolved in 80 % ethanol, 20 % (glacial) acetic acid at a concentration of 0.03 % overnight. The embryos were then de-stained by two thirty minute washes in 70 % ethanol and then incubated them in 95 % ethanol overnight. The embryos were pre-cleared in a 1 % potassium hydroxide (KOH) (Fisher Scientific 1310–58-3) solution for one hour. Embryos were then placed in a 0.005 % alizarin red (Sigma A5533) dissolved in 1% KOH overnight. The embryos were then placed in a 50 % glycerol (Fisher 56-81-5): 50 % (1 %) KOH solution until clear. The average time was one week to become fully cleared. Once cleared, the embryos were then placed in 100% glycerol for long-term storage and imaging. Skeletal preparations were imaged Leica MZ16F stereoscope and Leica DFC490 camera with Leica software.

Cell Proliferation/Death Assay:

Mice were administered 250μg EdU in PBS/10g mouse weight by intraperitoneal injection one hour prior to sacrifice. Embryos were then collected and prepared for cryopreservation as stated above. EdU was detected using Click-iTEdU Alexa Fluor 488 Imaging Kit

(Invitrogen #C10337) according to manufacturer's protocol. Images were captured using the Olympus BX60 microscope and Olympus DP70 digital camera using DC controller software. The percent of EdU positive cells was quantified using ImageJ/Fiji. Cell death was detected using activated Caspase-3 (stated previously) by immunofluorescence. For quantification, images were converted to 8-bit and background was removed with a 10 pixel "rolling ball". A signal threshold was auto set. Individual cells were determined using "watershed" and cells were then counted using "count particles".

Retinoic acid signaling activation and inhibition:

At-RA (Sigma R2625) was reconstituted in DMSO at 100mg/ml and diluted in peanut oil, and administered at 100μg/gm of body weight by oral gavage on E9.5 or E10.0. BMS-453 (Cayman Chemical, #19076) was administered by oral gavage to pregnant dams carrying embryos at E8.5, E9.5, E11.5, E13.5, and E15.5. BMS-453 was reconstituted in DMSO at 10μg/μl, diluted in corn oil, and administered at 3.5μg/gm or 5μg/gm of body weight of mouse. For oral gavage on day of tamoxifen administration, the corn oil used to dilute also contained tamoxifen.

Statistics:

All graphs and statistical analysis were generated using Prism 6 (GraphPad Software). Data are presented as mean ± SEM in all graphs. All pairwise sample comparisons were performed using a Mann-Whitney test. The p-values for statistical tests in all figures are represented as: * = $P < 0.05$, ** = $P < 0.01$, and *** = $P < 0.001$.

Supplementary Material

Refer to Web version on PubMed Central for supplementary material.

Acknowledgments:

Thanks to previous and current members of the Atit laboratory, Drs. Veronique Lefebvre, Edward Greenfield, and Clay Spencer for excellent discussion and advice. We thank Sai Thulabandu for his assistance with mouse work and experiments. We thank Gregg DiNuoscio for genotyping, immunostaining, and technical assistance, and Samuel Pan and Vidhi Mendpara for their assistance with sectioning tissues. We thank Bryan Hausman in the CWRU Orthopedics department for microCT imaging. We thank the CWRU SOM Light Microscopy Core Facility.

Funding: This work was supported by the following grants: NIH National Institute of Dental and Craniofacial Research R01 DE-01870 (R.P.A.), National Institutes of Health (NIH) T32 AR-007505 (J.F.), the Case Western Reserve University ENGAGE (M.D.) and SOURCE Programs (M.D.), and NIH Grant S10-OD016164 (CWRU SOM Light Microscopy Core Facility).

References:

Abe M, Maeda T **and** Wakisaka S (2008). Retinoic acid affects craniofacial patterning by changing Fgf8 expression in the pharyngeal ectoderm. Dev. Growth Differ 50, 717–729. [PubMed: 19046160] **and**

Abzhanov A, Rodda SJ, McMahon AP **and** Tabin CJ (2007). Regulation of skeletogenic differentiation in cranial dermal bone. Development 134, 3133–3144. [PubMed: 17670790] **and**

Alexandre D, Clarke JDW, Oxtoby E, Yan Y-L, Jowett T **and** Holder N (1996). Ectopic expression of Hoxa-1 in the zebrafish alters the fate of the mandibular arch neural crest and phenocopies a retinoic acid-induced phenotype. Development 122, 735–746. [PubMed: 8631251] **and**

Alon U (2007). Network motifs: theory and experimental approaches. Nature Rev Genetics 8, 450–461. [PubMed: 17510665]

Atit R, Sgaier SK, Mohamed OA, Taketo MM, Dufort D, Joyner AL, Niswander L **and** Conlon RA (2006). β-Catenin Activation Is Necessary and Sufficient To Specify the Dorsal Dermal Fate in the Mouse. Dev. Biol 296, 164–176. [PubMed: 16730693] **and**

Balmer JE **and** Blomhoff R (2002). Gene expression regulation by retinoic acid. J. Lipid Res 43, 1773–808. [PubMed: 12401878]

Basu S, Mehreja R, Thiberge S, Chen MT **and** Weiss R (2004) Spatiotemporal control of gene expression with pulse-generating networks. Proc. Natl. Acad.Sci. USA 101, 6355–6360. [PubMed: 15096621] **and**

Boylan JF, Lohnes D, Taneja R, Chambon P **and** Gudas LJ (1993). Loss of retinoic acid receptor gamma function in F9 cells by gene disruption results in aberrant Hoxa-1 expression and differentiation upon retinoic acid treatment. Proc. Natl. Acad. Sci. U. S. A 90, 9601–5. [PubMed: 8105479] **and**

Boylan JF, Lufkin T, Achkar CC, Taneja R, Chambon P **and** Gudas LJ (1995). Targeted disruption of retinoic acid receptor alpha (RAR alpha) and RAR gamma results in receptor-specific alterations in retinoic acid-mediated differentiation and retinoic acid metabolism. Mol. Cell. Biol 15, 843–51. [PubMed: 7823950] **and**

Bracken AP, Dietrich N, Pasini D, Hansen KH **and** Helin K (2006). Genome-wide mapping of polycomb target genes unravels their roles in cell fate transitions. Genes Dev 20, 1123–1136. [PubMed: 16618801] **and**

Carroll LS **and** Capecchi MR (2015). HOXC8 initiates an ectopic mammary program by regulating Fgf10 and Tbx3 expression, and Wnt/β-catenin signaling. Development dev 128298-.

Charité J, McFadden DG **and** Olson EN (2000). The bHLH transcription factor dHAND controls Sonic hedgehog expression and establishment of the zone of polarizing activity during limb development. Development 127, 2461–2470. [PubMed: 10804186] **and**

Chen JY, Penco S, Ostrowski J, Balaguer P, Pons M, Starrett JE, Reczek P, Chambon, **and** Gronemeyer H (1995). RAR-specific agonist/antagonists which dissociate transactivation and AP1 transrepression inhibit anchorage-independent cell proliferation. EMBO J 14, 1187–1197. [PubMed: 7720709] **and**

Chung SSW, Wang X, Roberts SS, Griffey SM, Reczek PR **and** Wolgemuth DJ (2011). Oral administration of a retinoic acid receptor antagonist reversibly inhibits spermatogenesis in mice. Endocrinology 152, 2492–2502. [PubMed: 21505053] **and**

Creuzet S, Couly G, Vincent C **and** Le Douarin NM (2002). Negative effect of Hox gene expression on the development of the neural crest-derived facial skeleton. Development 129, 4301–4313. [PubMed: 12183382] **and**

Dorsky RI, Moon RT **and** Raible DW (2000). Environmental signals and cell fate specification in premigratory neural crest. BioEssays 22, 708–16. [PubMed: 10918301] **and**

Dudakovic A, Camilleri ET, Xu F, Riester SM, McGee-Lawrence ME, Bradley EW, Paradise CR, Lewallen EA, Thaler R, Deyle DR, et al. (2015). Epigenetic control of skeletal development by the histone methyltransferase Ezh2. J. Biol. Chem 290, 27604–27617. [PubMed: 26424790]

Feldkamp LA, Davis LC **and** Kress JW (1984). Practical cone-beam algorithm. J. Opt. Soc. Am. A 1, 612–619.**and**

Ferguson J, Devarajan M, DiNuoscio G, Saiakhova A, Liu C-F, Lefebvre V, Scacheri P **and** Atit RP (2017). PRC2 is Dispensable in Vivo for β-Catenin-Mediated Repression of Chondrogenesis in Mouse Embryonic Cranial Mesenchyme. G3: Genes|Genomes|Genetics 8, g3.300311.2017.**and**

Firulli BA, Krawchuk D, Centonze VE, Vargesson N, Virshup DM, Conway SJ, Cserjesi P, Laufer E **and** Firulli AB (2005). Altered Twist1 and Hand2 dimerization is associated with Saethre-Chotzen syndrome and limb abnormalities. Nat. Genet 37, 373–81. [PubMed: 15735646] **and**

Funato N, Chapman SL, McKee MD, Funato H, Morris JA, Shelton JM, Richardson JA **and** Yanagisawa H (2009). Hand2 controls osteoblast differentiation in the branchial arch by inhibiting DNA binding of Runx2. Development 136, 615–625. [PubMed: 19144722] **and**

Galli A, Robay D, Osterwalder M, Bao X, Bénazet JD, Tariq M, Paro R, Mackem S **and** Zeller R (2010). Distinct roles of Hand2 in initiating polarity and posterior Shh expression during the onset of mouse limb bud development. PLoS Genet 6,.**and**

Gibson WT, Hood RL, Zhan SH, Bulman DE, Fejes AP, Moore R, Mungall AJ, Eydoux P, Babul-Hirji R, An J, et al. (2012). Mutations in EZH2 cause weaver syndrome. Am. J. Hum. Genet 90, 110–118. [PubMed: 22177091]

Goodnough LH, Chang A, Treloar C, Yang J, Scacheri PC **and** Atit RP (2012). Twist1 mediates repression of chondrogenesis by β-catenin to promote cranial bone progenitor specification. Development 139, 4428–4438. [PubMed: 23095887] **and**

Graf D, Malik Z, Hayano S **and** Mishina Y (2016). Common mechanisms in development and disease: BMP signaling in craniofacial development. Cytokine Growth Factor Rev 27, 129–139. [PubMed: 26747371] **and**

Grammatopoulos G. a, Bell E, Toole L, Lumsden a **and** Tucker a S. (2000). Homeotic transformation of branchial arch identity after Hoxa2 overexpression. Development 127, 5355–5365. [PubMed: 11076757] **and**

Han J, Ishii M, Bringas P, Maas RL, Maxson RE **and** Chai Y (2007). Concerted action of Msx1 and Msx2 in regulating cranial neural crest cell differentiation during frontal bone development. Mech. Dev 124, 729–745. [PubMed: 17693062] **and**

Hill J, Clarke JDW, Vargesson N, Jowett T **and** Holder N (1995). Exogenous retinoic acid causes specific alterations in the development of the midbrain and hindbrain of the zebrafish embryo including positional respecification of the Mauthner neuron. Mech. Dev 50, 3–16. [PubMed: 7605750] **and**

Ho TV, Iwata J, Ho HA, Grimes WC, Park S, Sanchez-Lara PA **and** Chai Y (2015). Integration of comprehensive 3D microCT and signaling analysis reveals differential regulatory mechanisms of craniofacial bone development. Dev. Biol 400, 180–190. [PubMed: 25722190] **and**

Hunt P, Gulisano M, Cook M, Sham MH, Faiella A, Wilkinson D, Boncinelli E **and** Krumlauf R (1991). A distinct Hox code for the branchial region of the vertebrate head. Nature 353, 861–4. [PubMed: 1682814] **and**

Ishii M, Sun J, Ting MC **and** Maxson RE (2015). The Development of the Calvarial Bones and Sutures and the Pathophysiology of Craniosynostosis 1st ed. Elsevier Inc.**and**

Jiang X, Iseki S, Maxson RE, Sucov HM **and** Morriss-Kay GM (2002). Tissue origins and interactions in the mammalian skull vault. Dev. Biol 241, 106–16. [PubMed: 11784098] **and**

Karsenty G (2008). Transcriptional Control of Skeletogenesis. Annu. Rev. Genomics Hum. Genet 9, 183–196. [PubMed: 18767962]

Karsenty G **and** Wagner EF (2002). Reaching a genetic and molecular understanding of skeletal evelopment. Dev. Cell 2, 389–406. [PubMed: 11970890]

Kochhar DM, Jiang H, Penner JD, Johnson AT **and** Chandraratna RA **.** (1998). The use of a retinoid receptor antagonist in a new model to study vitamin A-dependent developmental events. Int. J. Dev. Biol 42, 601–608. [PubMed: 9694631] **and.**

Komori T, Yagi H, Nomura S, Yamaguchi A, Sasaki K, Deguchi K, Shimizu Y, Bronson R , Gao Y-H, Inada M, et al. (1997). Targeted Disruption of Cbfa1 Results in a Complete Lack of Bone Formation owing to Maturational Arrest of Osteoblasts. Cell 89, 755–764. [PubMed: 9182763]

Krispin S, Nitzan E, Kassem Y **and** Kalcheim C (2010). Evidence for a dynamic spatiotemporal fate map and early fate restrictions of premigratory avian neural crest. Development 137, 585–595. [PubMed: 20110324] **and**

Krumlauf R (1994). Hox genes in vertebrate development. Cell 78, 191–201. [PubMed: 7913880]

Kumar S **and** Duester G (2014). Retinoic acid controls body axis extension by directly repressing Fgf8 transcription. Development 141, 2972–2977. [PubMed: 25053430]

Lee Y, Lee J-Y **and** Kim MH (2014). PI3K/Akt pathway regulates retinoic acid-induced Hox gene expression in F9 cells. Dev. Growth Differ 56, 518–25. [PubMed: 25212816] **and**

Liu L, Liu X, Ren X, Tian Y, Chen Z, Xu X, Du Y, Jiang C, Fang Y, Liu Z, et al. (2016). Smad2 and Smad3 have differential sensitivity in relaying TGFβ signaling and inversely regulate early lineage specification. Sci. Rep 6, 21602. [PubMed: 26905010]

Lohnes D, Mark M, Mendelsohn C, Dolle P, Dierich A, Gorry P, Gansmuller A **and** Chambon P (1994). Function of the retinoic acid receptors (RARs) during development (I). Craniofacial and skeletal abnormalities in RAR double mutants. Development 120, 2723– 2748. [PubMed: 7607067] **and**

Lund AH **and** Van Lohuizen M (2004). Polycomb complexes and silencing mechanisms. Curr. Opin. Cell Biol 16, 239–246. [PubMed: 15145347]

Maclean G, Dollé P **and** Petkovich M (2009). Genetic disruption of CYP26B1 severely affects development of neural crest derived head structures, but does not compromise hindbrain patterning. Dev. Dyn 238, 732–745. [PubMed: 19235731] **and**

Matt N, Ghyselinck NB, Wendling O, Chambon P **and** Mark M (2003). Retinoic acid-induced developmental defects are mediated by RARbeta/RXR heterodimers in the pharyngeal endoderm. Development 130, 2083–93. [PubMed: 12668623] **and**

Minoux M, Holwerda S, Vitobello A, Kitazawa T, Kohler H, Stadler MB **and** Rijli FM (2017a). Gene bivalency at Polycomb domains regulates cranial neural crest positional identity. Science (80-.) 355, eaal2913.**and**

Minoux M, Holwerda S, Vitobello A, Kitazawa T, Kohler H, Stadler MB **and** Rijli FM (2017b). Gene bivalency at Polycomb domains regulates cranial neural crest positional identity. Science 355, eaal2913. [PubMed: 28360266] **and**

Mirzamohammadi F, Papaioannou G, Inloes JB, Rankin EB, Xie H, Schipani E, Orkin SH **and** Kobayashi T (2016). Polycomb repressive complex 2 regulates skeletal growth by suppressing Wnt and TGF-β signalling. Nat. Commun 7, 12047. [PubMed: 27329220] **and**

Moosa S **and** Wollnik B (2016). Altered FGF signalling in congenital craniofacial and skeletal disorders. Semin. Cell Dev. Biol 53, 115–125. [PubMed: 26686047]

Morkmued S, Laugel-Haushalter V, Mathieu E, Schuhbaur B, Hemmerlï¿½ J, Dollï¿½ P, Bloch-Zupan A **and** Niederreither K (2017). Retinoic acid excess impairs amelogenesis inducing enamel defects. Front. Physiol 7, 1–14.**and**

Nakashima K, Zhou X **and** Al. GK **et** (2002). The novel zinc fingercontaining transcription factor Osterix is required for osteoblast 12 BioMed Research International differentiation and bone formation. Cell 108, 17–29. [PubMed: 11792318] **andet**

Nishio Y, Dong Y, Paris M, O'Keefe ,RJ, Schwarz ,EM and Drissi H (2006). Runx2-mediated regulation of the zinc finger Osterix/Sp7 gene. Gene 372, 62–70. [PubMed: 16574347]

Ornitz DM **and** Marie PJ (2002). FGF signaling pathways in endochondral and intramembranous bone development and human genetic disease. Genes Dev 16, 1446– 1465. [PubMed: 12080084]

Pfaff MJ, Xue K, Li L, Horowitz MC, Steinbacher DM **and** Eswarakumar JVP (2016). FGFR2c-mediated ERK-MAPK activity regulates coronal suture development. Dev. Biol 415, 242–250. [PubMed: 27034231] **and**

Rivera-Perez JA, Wakamiya M **and** Behringer RR (1999). Goosecoid acts cell autonomously in mesenchyme-derived tissues during craniofacial development. Development 126, 3811–3821. [PubMed: 10433910] **and**

Rivers LE, Young KM, Rizzi M, Jamen F, Psachoulia K, Wade A, Kessaris N **and** Richardson WD (2008). PDGFRA/NG2 glia generate myelinating oligodendrocytes and piriform projection neurons in adult mice. Nat. Neurosci 11, 1392–1401. [PubMed: 18849983] **and**

Roybal PG, Wu NL, Sun J, Ting M chun, Schafer CA **and** Maxson RE (2010). Inactivation of Msx1 and Msx2 in neural crest reveals an unexpected role in suppressing heterotopic bone formation in the head. Dev. Biol 343, 28–39. [PubMed: 20398647] **and**

Satokata I **and** Maas R (1994). Msx1 deficient mice exhibit cleft palate and abnormalities of craniofacial and tooth development. Nat. Genet 6, 348–356. [PubMed: 7914451]

Satokata I, Ma L, Ohshima H, Bei M, Ian W, Nishizawa K, Maeda T, Takano Y, Uchiyama M, Heaney S, et al. (2000). Msx2 deficiency in mice causes pleiotropic defects in bone growth and ectodermal organ formation. Nat. Genet 24, 391–395. [PubMed: 10742104]

Savory JGA, Edey C, Hess B, Mears AJ **and** Lohnes D (2014). Identification of novel retinoic acid target genes. Dev. Biol 395, 199–208. [PubMed: 25251699] **and**

Schilling TF **and** Kimmel CB (1994). Segment and cell type lineage restrictions during pharyngeal arch development in the zebrafish embryo. Development 120, 483–94. [PubMed: 8162849]

Schindelin J, Arganda-Carreras I, Frise E, Kaynig V, Longair M, Pietzsch T, Preibisch S, Rueden C, Saalfeld S, Schmid B, et al. (2012). Fiji: an open-source platform for biological-image analysis. Nat. Methods 9, 676–82. [PubMed: 22743772]

Schmittgen TD **and** Livak KJ (2008). Analyzing real-time PCR data by the comparative CT method. Nat. Protoc 3, 1101–1108. [PubMed: 18546601]

Schneider C, Rasband WS **and** Eliceiri KW (2012). NIH Image to ImageJ: 25 years of image analysis. Nat. Methods 9, 671–675. [PubMed: 22930834] **and**

Schuettengruber B, Bourbon HM, Di Croce L **and** Cavalli G (2017). Genome Regulation by Polycomb and Trithorax: 70 Years and Counting. Cell 171, 34–57. [PubMed: 28938122] **and**

Schwarz D, Varum S, Zemke M, Schöler A, Baggiolini A, Draganova K, Koseki H, Schübeler D **and** Sommer L (2014). Ezh2 is required for neural crest-derived cartilage and bone formation. Development 141, 867–77. [PubMed: 24496623] **and**

Shen X, Liu Y, Hsu YJ, Fujiwara Y, Kim J, Mao X, Yuan GC **and** Orkin SH (2008). EZH1 Mediates Methylation on Histone H3 Lysine 27 and Complements EZH2 in Maintaining Stem Cell Identity and Executing Pluripotency. Mol. Cell 32, 491–502. [PubMed: 19026780] **and**

Simon J. a **and** Kingston RE (2009). Mechanisms of polycomb gene silencing: knowns and unknowns. Nat. Rev. Mol. Cell Biol 10, 697–708. [PubMed: 19738629]

Tatton-Brown K, Hanks S, Ruark E, Zachariou A, Duarte SDV, Ramsay E, Snape K, Murray A, Perdeaux ER, Seal S, et al. (2011). Germline mutations in the oncogene EZH2 cause Weaver syndrome and increased human height. Oncotarget 2, 1127–33. [PubMed: 22190405]

Trainor PA **and** Krumlauf R (2001). Hox genes, neural crest cells and branchial arch patterning. Curr. Opin. Cell Biol 13, 698–705. [PubMed: 11698185]

Tran TH, Jarrell A, Zentner GE, Welsh A, Brownell I, Scacheri PC **and** Atit R (2010). Role of canonical Wnt signaling/β-catenin via Dermo1 in cranial dermal cell development. Development 137, 3973–3984. [PubMed: 20980404] **and**

Williams SS, Mear JP, Liang H-C, Potter SS, Aronow BJ **and** Colbert MC (2005). Large-scale reprogramming of cranial neural crest gene expression by retinoic acid exposure. Physiol. Genomics 19, 184–197.**and**

Yan G, Tian J, Zhu S, Dai Y **and** Qin C (2008). Fast cone-beam CT image reconstruction using GPU hardware. J. Xray. Sci. Technol 16, 225–234.**and**

Yoshida T, Vivatbutsiri P, Morriss-Kay G, Saga Y **and** Iseki S (2008). Cell lineage in mammalian craniofacial mesenchyme. Mech. Dev 125, 797–808. [PubMed: 18617001] **and**

Zhao X, Sirbu IO, Mic FA, Molotkova N, Molotkov A, Kumar S **and** Duester G (2009). Retinoic Acid Promotes Limb Induction through Effects on Body Axis Extension but Is Unnecessary for Limb Patterning. Curr. Biol 19, 1050–1057. [PubMed: 19464179] **and**

Highlights:

- *Ezh2* is required in a development stage-specific manner in the mouse cranial mesenchyme to promote calvarial bone lineage commitment.
- RA signaling inhibitors can partially rescue the loss of calvarial bones in *Ezh2* mutants
- *Ezh2* is required to suppress the expression of anti-osteogenic factors which are poised to be induced by Retinoic acid signaling in an incoherent type-1 feedforward loop(I1-FFL).

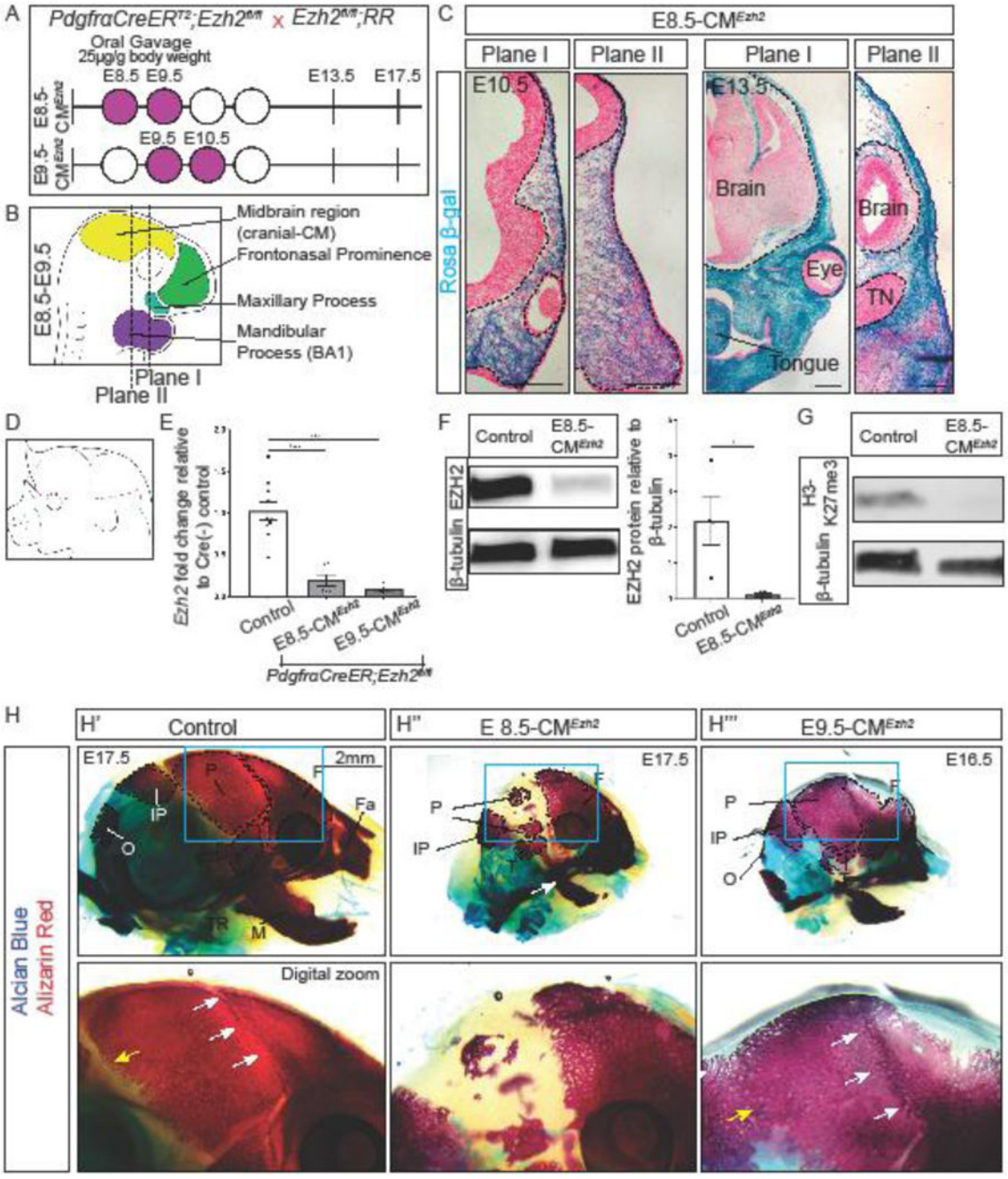

Figure 1: Inducible and conditional deletion of *Ezh2* at E8.5 in both the CNCC-derived and PM-derived CM.

(A) Mating strategy and gavage regimen for conditional *Ezh2* deletion for E8.5-CM^{Ezh2} and E9.5-CM^{Ezh2} mutants. Tamoxifen was administered by oral gavage starting at E8.5 or E9.5 (purple shaded) at a concentration of 25µg/g mouse body weight. (B) Anatomy of mouse embryo between E8.5 and E9.5. *PdgfraCreER* is active in the CM, frontonasal prominence, maxillary process, and BA1. Plane I corresponds to the future frontal bone, and plane II corresponds to the future parietal bone. (C) *PdgfraCreER/+;Ezh2$^{fl/fl}$* Rosa 26 Reporter lineage-marked CM in coronal sections. E8.5+E9.5 gavages is sufficient to induce Cre-ER

recombination in cranial mesenchyme in frontal bone and parietal bone primordia in plane I and plane II, respectively (scale bar = 200μm). (D) Schematic representing manual enrichment of the cranial mesenchyme (CM). The ectoderm was manually removed and all the CM above the eye was collected. (E) RT-qPCR for *Ezh2* in the manually enriched CM at E13.5. (F) Western blot for EZH2 in the manually enriched cranial mesenchyme. Band intensities were quantified using ImageJ/Fiji. (G) Western blot for H3K27me3 in manually enriched CM. (H) Whole mount skeletal staining of controls and E8.5-CM^{Ezh2} and E9.5-CM^{Ezh2} mutants at E17.5. All embryos were imaged at the same magnification. White arrows mark the coronal suture and yellow arrow marks the lambdoid suture. F = frontal bone; P = parietal bone; T= temporal; IP = interparietal bone; O = occipital bone; Fa = facial bones; M = mandible, Tympanic ring = TR; TN = Trigeminal neurons.

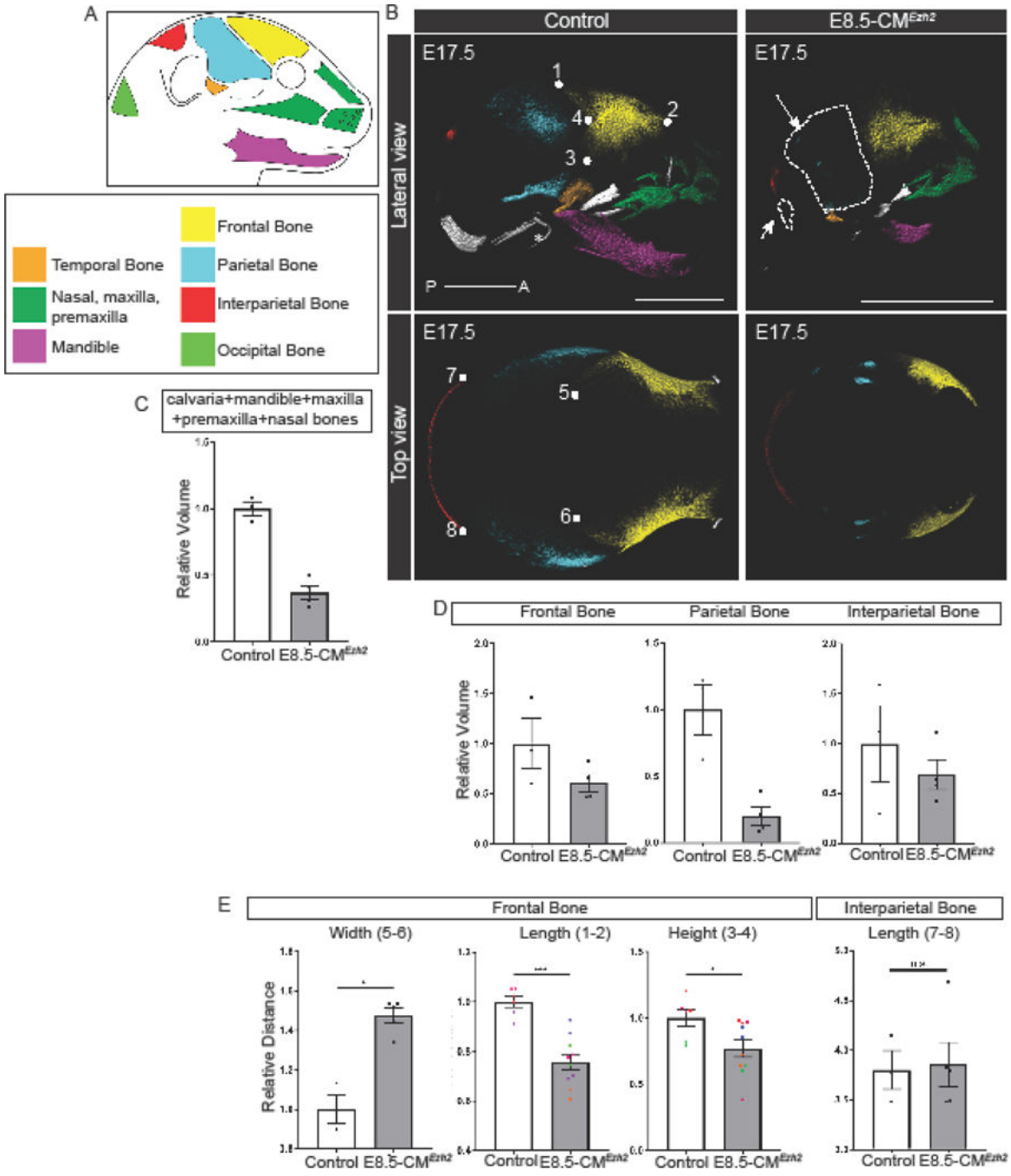

Figure 2: E8.5-CM^{Ezh2} leads to truncation of CNCC-derived bones and a severe reduction in PM-derived bones.

(A) Schematic and key representing the primary bones examined in E8.5-CM^{Ezh2} embryos. (B) Psuedo-colored 3D images from microCT at E17.5 of E8.5-CM^{Ezh2} embryos. * indicates ear bones which are lost in the mutants. Arrows point to the reduced/lost PM-derived bones. Numbers represent landmarks used for morphometric measurements (scale bar = 2mm). (C) Quantification of changes in combined bone volume of the calvaria, mandible, maxilla, premaxilla, and nasal bones. (D) Quantification of changes in bone volume in the bones of the calvaria. (E) Morphometric analysis of the frontal and

interparietal bone. Both the left and right frontal bones were measured and plotted. Pairs of colored dots correspond with each left-right pair. Definition of landmarks: (1,5,6) Most posterior-superior point of the frontal bone (2) Most anterior-superior point of the frontal bone (3) Most posterior-inferior point of the frontal bone (4) Most posterior-lateral intersection of the frontal and parietal bone (7,8) Lateral points of the parietal bone.

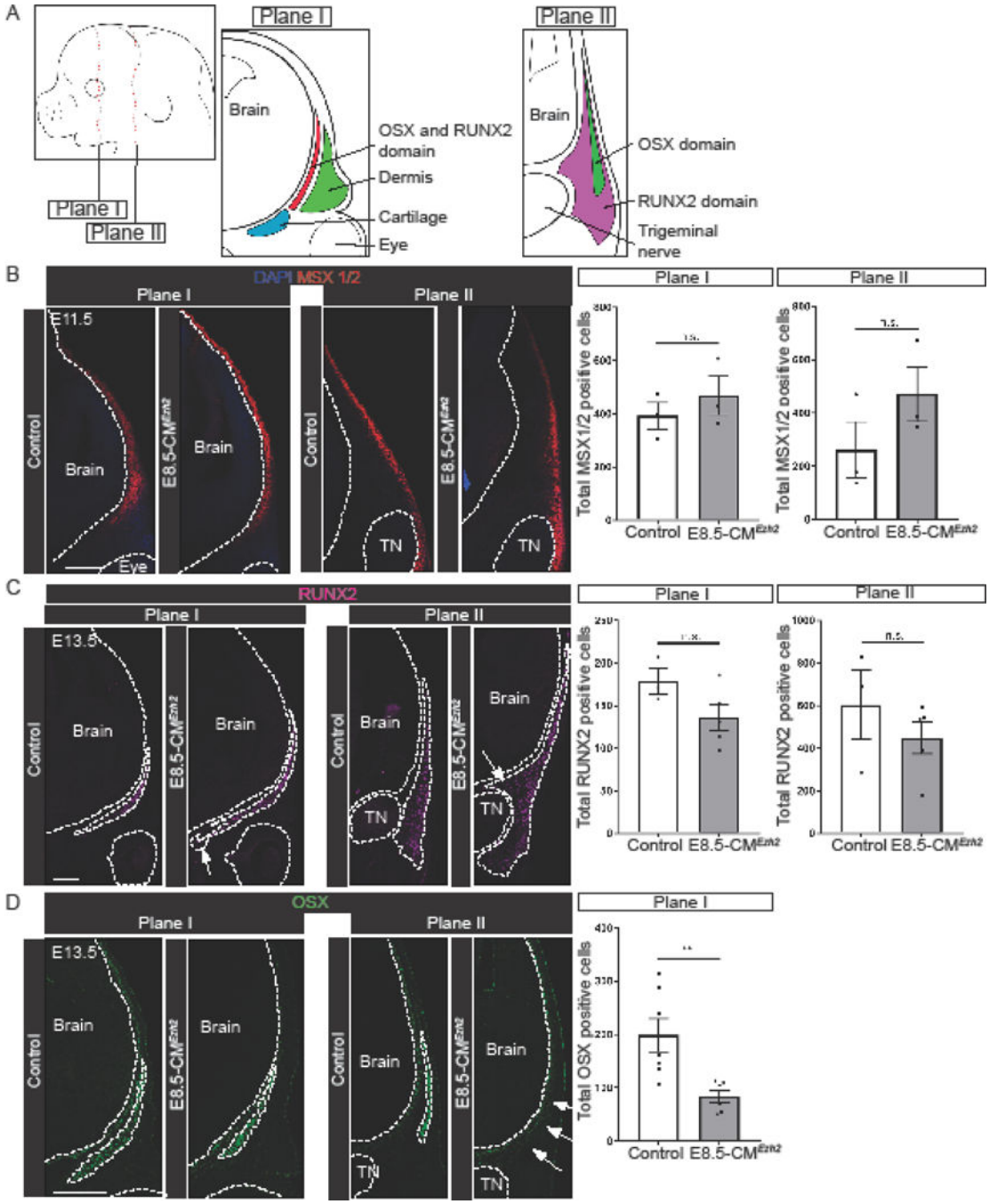

Figure 3: Arrest during bone differentiation in PM-derived parietal bone in E8.5-CM^{Ezh2} mutants.

(A) Schematic of E13.5 mouse embryo and coronal sections. Plane I refers to future frontal bone and plane II refers to future parietal bone. (B) Immunofluorescence of bone precursor marker MSX1/2 in E11.5 coronal sections. Quantification of total number of cells positive for MSX1/2 in plane I and plane II. (C) Immunofluorescence for bone progenitor marker RUNX2 in E13.5 coronal sections. Arrows indicate expanded domains. Quantification of total number of cells positive for RUNX2 in plane I and plane II. (D) Immunofluorescence for bone progenitor marker OSX in E13.5 coronal sections. Arrows indicate lost expression

in plane II. Quantification for total number of cells positive for OSX in plane I. Quantification in plane II was not performed due to lost expression in the mutant. TN: Trigeminal nerve. Scale bars = 200μm.

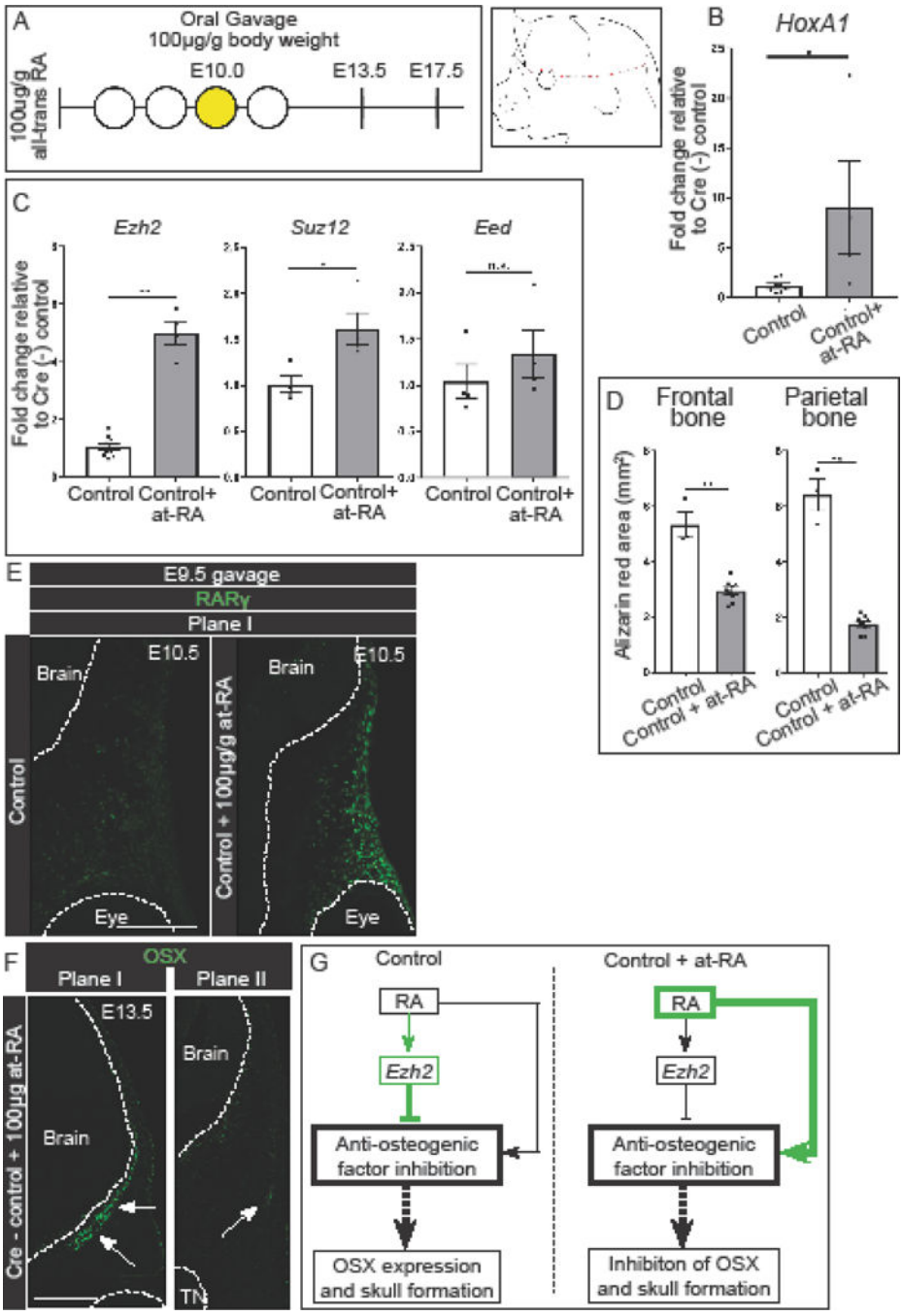

Figure 4: Activation of retinoic acid signaling inhibits skull bone formation and positively regulates Ezh2.

(A) Gavage regimen for at-RA (yellow shaded) in cre- control embryos and schematic for obtaining manually enriched E13.5 CM. At-RA was administered at E10.0. (B) Up regulation of known RA-signaling target, HoxA1, in manually enriched E13.5 CM. (C) Expression levels of PRC2 components in manually enriched CM. (D) Quantification of total area of the frontal and parietal bones in E17.5 skeletal staining. (E) Immunofluorescence for RARγ in the frontal bone primordia of E10.5 at-RA treated cre- control embryos. Embryos were administered at-RA at E9.5. (F) Immunofluorescence for

OSX in the frontal and parietal bone primordia of at-RA treated embryos. At-RA was administered at E9.5. White arrows mark OSX+ domain. (G) Summary of the regulation of skull bone formation by *Ezh2* and at-RA by which *Ezh2* maintain a balance of activation and suppression of anti-osteogenic genes. Following administration of at-RA, the balance is shifted towards activation of anti-osteogenic genes.

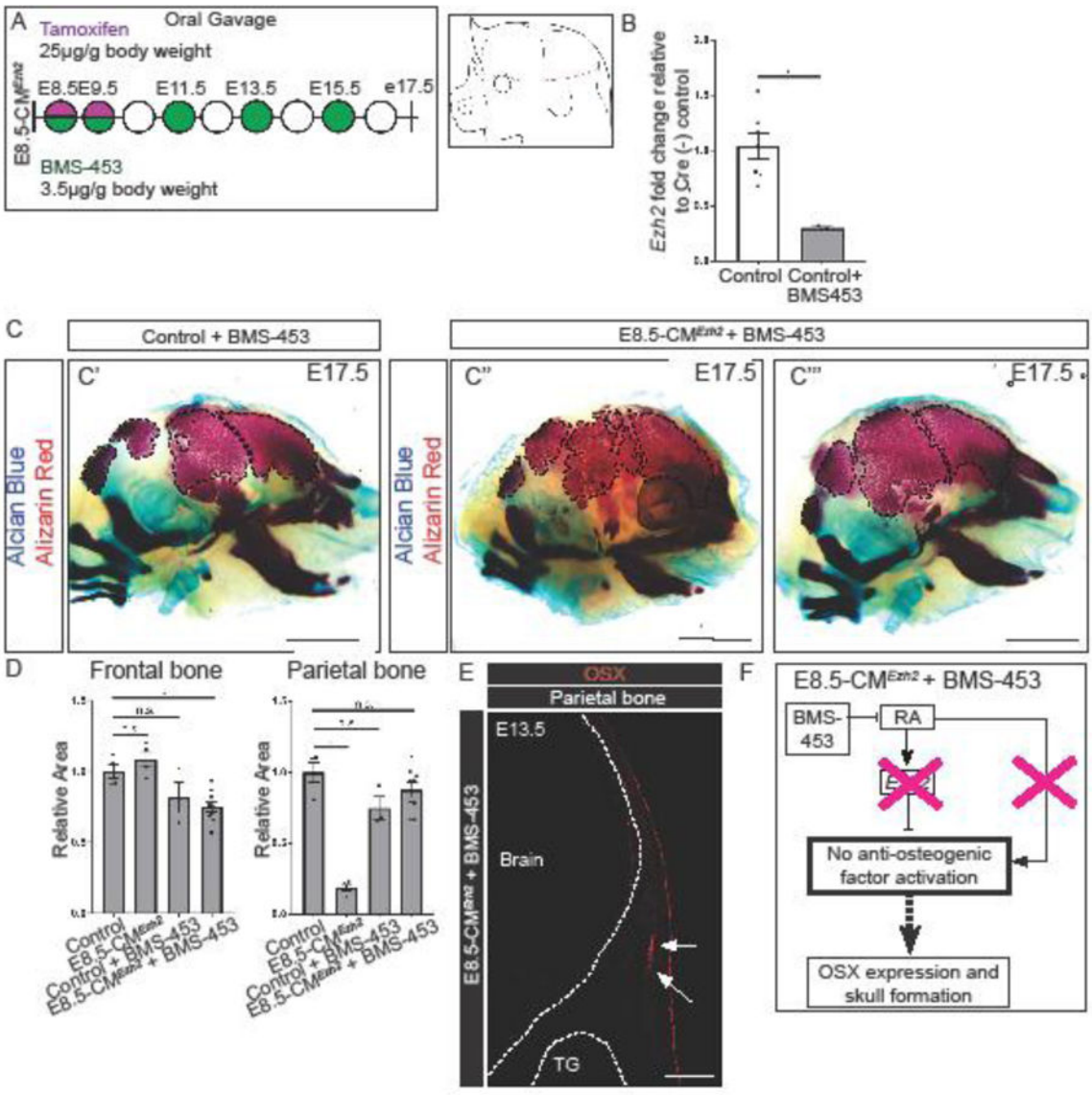

Figure 5: Pharmacological inhibition of RA signaling partially rescues the E8.5-CM*Ezh2* mutant phenotype and restores the PM-derived bones.

(A) Gavage regimen for tamoxifen and RA-antagonist BMS-453 in E8.5-CM*Ezh2* mutants and schematic of obtaining manually enriched CM without the ectoderm. (B) RT-qPCR for *Ezh2* in *Cre*- control and BMS-453 treated embryos from E13.5 manually enriched CM. (C) Skeletal staining of E17.5 3.5µg/gm BMS-453 treated *Ezh2* mutants. C' and C'' represent two different litters. Alcian blue marks cartilage and alizarin red marks bone (scale bar = 2mm). (D) Quantification of the Alizarin Red stained area outlined in (C) using ImageJ/Fiji. (E) Immunofluorescence of OSX in the parietal bone at E13.5. Arrows indicate partial restoration of OSX (scale bar = 200µm). (F) Schematic with proposed model by which, in the absence of *Ezh2,* inhibition of RA-signaling prevents the activation of the anti-osteogenic genes restoring OSX expression and skull bone formation.

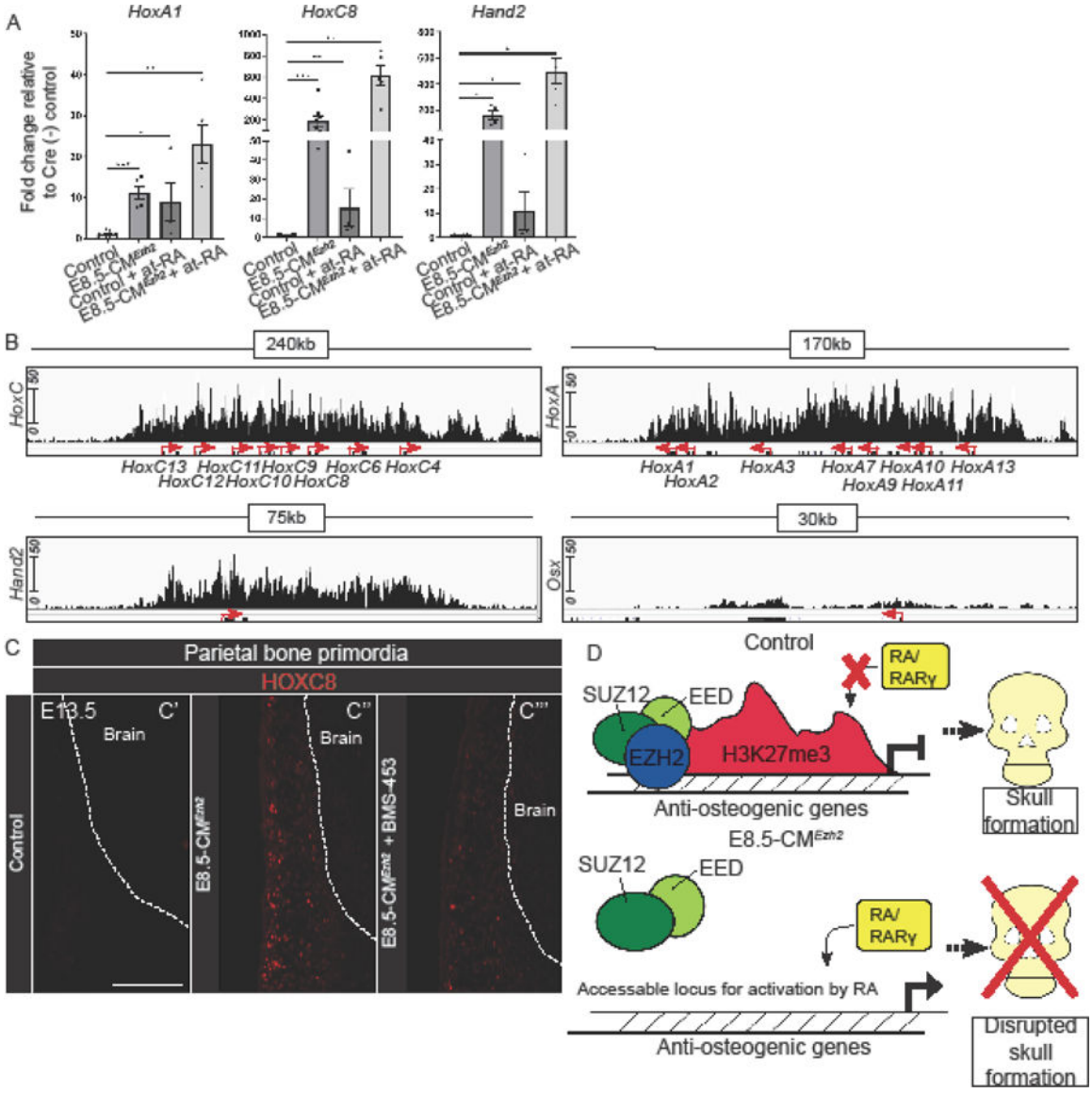

Figure 6: Ezh2 and RA-signaling maintain a balance of anti-osteogenic genes in the CM.

(A) Relative mRNA quantity for *HoxA1, HoxC8* and *Hand2* expression levels in E13.5 manually enriched CM in *Cre*- control, E8.5-CM^{Ezh2} mutant, 100μg/gm body weight at-RA exposure at E10.0 in *Cre*- control, and E8.5-CM^{Ezh2} mutants treated with 100μg/gm at-RA. (B) Integrated Genome Viewer representation of H3K27me3 ChiP-seqencing of E13.5 cranial mesenchyme control. (C) Protein expression of HOXC8 in in the parietal bone primordia of E13.5 control, E8.5-CM^{Ezh2}, and 3.5ug/gm body weight treated BMS-453 at E8.5, 9.5, and 11.5. embryo. Scale bars: 200μm. (D) Hypothetical model explaining that EZH2 and RA signaling balance the inhibition of anti-osteogenic factors to ensure calvarial bone commitment and development.